Kinetics of soot formation from benzene pyrolysis

T. Viola, L. Carneiro Piton, M.Idir, N. Chaumeix, A. Comandini
Institut de Combustion, Aérothermique, Réactivité et Environnement, CNRS-INSIS
Orleans, France

1 Abstract

Understanding soot formation is still a significant challenge for developing the next generation of environmentally friendly sustainable combustion systems. In this paper, a new detailed kinetic mechanism for soot formation under pyrolytic conditions is presented. The work was carried out at ICARE-CNRS by implementing a Python framework built for the automatic generation of kinetic mechanisms (SMAuG - Soot Mechanism Automated Generator) for the development of a model for solid-phase chemistry. Such model was combined with the gas-phase sub-mechanism developed in previous works and specifically dedicated to the formation of PAH products in single-pulse shock tube experiments from pyrolysis of fuel components and mixtures. In addition, an upgrade of PAHs chemistry was made through a new proposal of hybridized gas phase scheme with the contribution of polyynes chemistry, also implemented in the mechanisms of soot inception and surface growth. The kinetic model was validated against new laser-based shock tube experimental data on pyrolysis of benzene, key component in aromatic fuels and intermediate in soot formation, as well as against literature data.

2 Introduction

The formation of carbonaceous soot particles is a complex mechanism involving a process of multiple chemical and physical steps [1,2]. Such complexity poses serious limitations and questions in the possibility of developing sufficiently accurate soot models for the design of clean combustion systems through engines optimization and fuel re-formulation. Detailed soot kinetic models based on laboratory experiments have already been proposed in the past. Among them, the models based on the sectional method [3] have been popular for years as they offer the possibility of using lumped chemical species for an “apparently simplified” approach. The mechanism presented in this paper combines the gas-phase PAH chemistry from our previous works [4] with the new solid-phase chemistry mechanism, iincluding the PAH routes and the alternative pathways of soot formation via polyynes chemistry [5,6]. The mechanism was generated through the in-house developed python framework SMAuG (Soot Mechanism Automated Generator) which currently features the capability to generate detailed kinetic mechanisms applied to the soot formation chemistry in pyrolytic conditions. Experimental results on benzene pyrolysis were also obtained using conventional shock tube laser-based technique (soot volume fractions) for model validation. The model was also tested against relevant literature data.

Correspondence to: andrea.comandini@cnrs-orleans.fr

3 Experimental setup and chemical kinetic model.

To evaluate the performance of the proposed mechanism, the ICARE heated shock tube (HST), widely adopted for chemical kinetics at high temperatures and particularly for soot formation [7,8], was implemented to obtain experimental results on benzene pyrolysis. The shock tube driven section has a length of 5.15 m and an internal diameter of 52.4 mm. It is equipped with four pressure sensors (CHIMIE METAL A25L05B) positioned along the shock tube close to the end-wall at a distance of 150 mm from each other. The sensors signals are used to measure the velocity of the incident shock wave, extrapolated to the end wall, from which the thermodynamic conditions behind the reflected shock waves are then calculated by solving the conservation equations. The computed T_5 has a maximum error of 25-30 K due to the wave attenuation and the uncertainty in determining the exact positions of the pressure sensor sensitive surfaces. A PCB Piezotronics pressure sensor located at the end-wall of the driven section measures the pressure–time profiles. Signal acquisition is performed using three Rohde & Schwarz RTB 2004 oscilloscopes, which record pressure signals and data from the laser acquisition system. Laser extinction measurements for soot volume fractions quantification are carried out with a He:Ne laser @ λ=633nm. The detector is a HAMAMATSU R59838 photomultiplier tube. The soot volume fractions are calculated as in equation (1), where m is the complex refractive index of soot particles, l the length crossed by the incident beam (diameter of the shock tube), λ the wavelength of the transmitted beam, I_0 the intensity of the incident beam. The function of the refractive index is assumed to be 0.36 as used in previous works in the literature, e.g. [9,10]. The experiments were performed with 0.082% benzene in argon, pressures behind the reflected shock waves between 16.4–18.3 bar, and initial carbon concentrations of 3.06 – 3.90x10^{17} atoms/cm^3. A typical pressure profile is presented in Fig. 1.

$$f_v = \frac{\lambda}{6\pi l \,\mathrm{Im}\left(\frac{m^2-1}{m^2+2}\right)} \ln\frac{I}{I_0} \mathrm{m} \qquad \textit{Eqn 1: Soot volume fraction fv.}$$

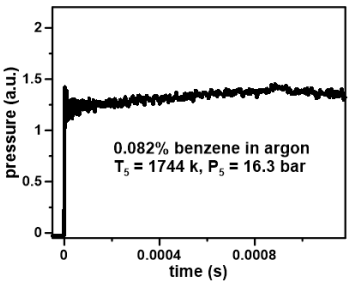

Figure 1. Typical PCB pressure profile.

The present kinetic mechanism is modeled on the concept of pseudo lumped species BINs along the lines of the CRECK mechanism scheme [11]. The framework SMAuG is capable of generating the mechanism (reaction and thermodynamics files in .dat, .CKI and .CKT, .cti, and .yaml) starting from defined chemical species (radicals, resonantly stabilized radicals, molecules, polyynes, BINs), reference reaction rate constant parameters for the different reaction classes. The kinetic parameters are entered by a dual system, i.e., from the launcher or from .csv files containing the input information. Reaction rate constant parameters are adjusted according to kinetic- or physical-type rate rules. These include the HACA mechanism responsible for activating the surfaces of the PAHs and BINs by H-abstraction with subsequent growth by carbon addition; the classes of soot inception PAHs+PAHs/PAHs+BINs and PYYNs+BINs, soot inception between BINs/BINs, surface growth, coalescence, and agglomeration. Molecule-molecule interactions from inception to aggregation are scaled according to [12]. The rate rule system was implemented from CRECK, with optimized reaction rate parameters based on the model validation, and extended to the PAHs+polyynes and polyynes+BINs reaction classes for radicals and molecules. Further tuning of the parameters was devoted for the interactions between small-resonantly-stabilized radicals (i.e. C_3H_3, C_5H_5, C_7H_7) and resonantly-stabilized PAHs. The optimized reference kinetic parameters are reported in Table 1.

Table 1. Reaction classes and reference rate parameters implemented in the current model. Units are in *mol cm s K cal*. Parameters for Arrhenius expression $k=A\cdot T^{n}\cdot\exp(-E_a/RT)$.

Reaction classes	*A*	*n*	*Ea*	*References*
H-abstraction				
$H+BIN_i \rightarrow H_2+BINJ_{i\ (i \le 3)}$	4.8E+6	2	10500	[11]
Carbon addition				
$C_xH_y+BINJ_i \rightarrow$ products $_{(i \le 3)}$	1.0E+12	0	5000	[11]
$C_xH_y+BINJ_i \rightarrow$ products $_{(i > 3)}$	1.0E+12	0	1000	[11]
Inception - gas-phase to large PAHs → products $BIN_{i\ (i < 5)}$				
$SRSR+PAH_r$	7.34E+63	-13.74	51540	[4]
$SRSR+PAH_m$	6.26E+9	2.61	56500	[4]
PAH_r+PAH_r	3.09E+12	0.036	1703	[4]
$PAH_{rsr}+PAH_{rsr}$	1.204E+39	-6.855	54539.3	[4]
PAH_r+PAH_m	5.73E+12	0	4305	[4]
$PAH_{mH}+PAH_{mH}$	1.0E+9	0.5	0	p.w
$PAH_{rsr}+PAH_r$	1.66E+64	-14.68	33262	[4]
$PAH_{rsr}+PAH_m$	4.0E+11	0	19000	[11]
$PAH_{rsr}+PYYN_r/PYYN_m$	1.0E+13	0	0	p.w
$PYYN_m+PAH_r$	2.0E+13	0	0	p.w
$PYYN_r+PAH_r$	4.0E+13	0	0	p.w
$PYYN_r+PAH_m$	2.0E+13	0	0	p.w
$C_2H_2+PYYN_r$	4.49E+82	-20.02	51830	p.w
$PAH_{mH}+PYYN_m$	1.5E+14	0	42700	[20]
Inception - PAHs/PYYNs → products $BIN_{i\ (i < 5)}$				
$SRSR+BINJ_i$	3.9E+13	-0.967	-3266.5	[4]
PAH_r+BINJ_i	3.0E+39	-6.855	54539.3	[4]
$PAH_{rsr}+BINJ_i$	6.0E+39	-11.108	38000	[4]
$SRSR+BIN_i$	7.83E+12	0.18	33550.0	[4]
$PAH_{rsr}+BIN_i$	1.0E+12	0	19000	[11]
PAH_r+BINJ_i	7.17E+39	-0.967	54539.3	[4]
PAH_r+BIN_i	7.16E+12	0	4305	[4]
PAH_m+BINJ_i	5.00E+13	0	32800	[4]
$PAH_{mH}+BIN_i$	2.50E+09	0.5	0	p.w
$PYYN_r+BINJ_i$	2.0E+14	0	0	p.w
$PYYN_m+BINJ_i$	4.0E+13	0	0	p.w
$PYYN_r+BIN_i$	2.0E+14	0	0	p.w
$C_2H_2+ BIN_i$	4.0E+13	0	31800	p.w
$PYYN_m+BIN_i$	1.5E+14	0	42700	[20]
Inception - BINs → products $BIN_{i\ (i,n < 5)}$				
$BINJ_i+BINJ_n$	4.0E+13	0	3000	p.w
BIN_i+BINJ_n	4.0E+13	0	6000	p.w
BIN_i+BIN_n	1.0E+9	0.5	0	p.w
Surface growth → products $BIN_{i\ (i \le 4 \text{ and } n \ge 5)}$				
$SRSR+BINJ_i$	6.26E+09	2.61	56500	[4]
$PAH_{rsr}+BINJ_i$	6.0E+12	0	0	p.w
PAH_r+BINJ_i	2.0E+13	0	0	p.w
PAH_m+BINJ_i	9.55E+11	0	0	[4]
$PYYN_r+BINJ_i$	2.0E+13	0	0	p.w
$PYYN_m+BINJ_i$	1.5E+13	0	0	p.w
$BINJ_i+BINJ_n$	1.0E+13	0.5	0	p.w
BIN_i+BINJ_n	5.0E+11	0.5	0	p.w
Coalescence and Aggregation→ products $BIN_{i\ (i, n \ge 5)}$				
$BINJ_i+BINJ_n$	4.0E+13	0.5	0	[11]
Dehydrogenation				
$BINJ_i \rightarrow H_2+BINJ_i$	1.0E+8	0	32000	[11]
$BINJ_i \rightarrow H\cdot+BIN_{i(i \le 3)}$	1.0E+11	0	12000	[11]
Demethylation				
$H\cdot+BINJ_i \rightarrow CH_3\cdot+$products	1.2E+13	0	5000	[11]
C–H fission/recombination				
$BIN_i \rightarrow H\cdot+BINJ_{i(i \le 3)}$	1.5E+17	0	114000	[11]
$H\cdot+BINJ_i \rightarrow BIN_{i(i \le 3)}$	1.0E+14	0	0	[11]

4. Results and discussion

The final model consists of about 850 chemical species and 35000 reaction. It can be used to predict and model soot through 0D simulations in isothermal and constant pressure batches or by evaluating constrained pressure conditions using experimental profiles of shock-tube experiments. The mechanism can be run on both Cantera [13] and Chemkin [14].

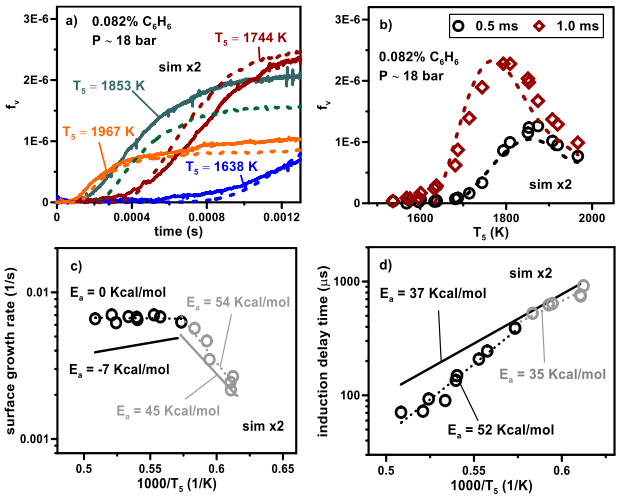

Figure 2. Experiment and simulations of 0.082% benzene in argon.

Figure 2 provides a global overview of the mechanism predictivity against the new experimental data of the present work (0.082% C_6H_6 in Ar). Figure 1a shows examples of soot volume fraction time-history at different temperature conditions. As expected by the common features of f_v profiles in shock-tube experiments, soot starts forming early at high temperatures, reaching its expected maximum around 1750 K before decreasing at lower temperatures. The model is capable to reproduce the quantitative values within a factor of 2, but more importantly it captures the qualitative profiles throughout the entire temperature range. The experimental profiles were also used to derive different kinetic parameters to be compared with the simulations for a more detailed characterization of the model capabilities. First, the soot volume fractions at fixed times (0.5 and 1.0 ms) are shown in Figure 2b. The modeling results are again multiplied by a factor 2. The experimental and modeling profiles are very similar, in particular the temperatures of the peak volume fractions at 0.5 ms coincide while there is a slight shift of around 30 K for the data at 1 ms. The relative experimental soot volume fractions at the two reaction times are well captured by the model. The soot growth rate can also be extracted from the f_v profiles as presented in Figure 2c. The experimental results clearly indicate two different regimes for lower or higher temperatures. The temperature threshold separating the two regimes is around 1750 K. The global activation energy of the growth below such temperature is around 54 kcal/mol, while above the growth rate is nearly constant. At all temperatures, the growth is mainly governed by BIN+BIN and BIN+polyyne reactions, as the benzene quickly decomposes to C_2H_2 and C_4H_2 triggering the polyyne routes. At temperatures below 1750 K, the reactions of BIN radicals with C_6H_6 and C_9H_7 provide a minor contribution to the surface growth. The model is capable to reproduce the experimental behavior. The simulated global activation energy of the soot surface growth below 1750 K is 45 kcal/mol, around 9 kcal/mol lower than the experimental value, while above 1750 K it is slightly negative. The growth rate at high temperature is underpredicted by a factor 1.3 on average. To be noted, the growth rate has been multiplied by a factor 2 as the simulations f_v. Regarding the induction delay times, defined as the time between the arrival of the shock wave at the end-wall and the time obtained by extrapolating the maximum slope of the f_v curve to the baseline, the experimental results have been divided into two parts as for the surface growth, with temperature limit around 1750 K (Figure 2d). At lower temperatures, the global activation energy of the induction process is around 35 kcal/mol, at higher temperatures it is around 52 kcal/mol. The modeling results are reasonable in terms of absolute induction values, although

they are characterized by a single slope similar to the one observed in the experiments below 1750 K. The global activation energy is around 37 kcal/mol (Figure 2d). The maximum discrepancy between the simulation and the experiments is a factor 2 at the highest temperature conditions (1967 K).

The comparison between the experimental induction delay times in the present work with those from literature studies at different initial carbon concentrations are reported in Figure 3a. The literature data from Drakon et al. [15] show the two slopes also presented in Figure 2d (up to 1750 K and between 1750 K and 2000 K). The authors also performed experiments at higher temperatures, above 2000 K, where the induction curve changes once again the slope. This behavior is somehow less evident but still present in the data by Vlasov et al. [16] concerning their experiments with the highest carbon atom concentrations. The present kinetic model is capable to reasonably well reproduce the data, especially for the data by Vlasov et al. [16] (Figure 3b). The simulation results confirm better agreement with the data in the low-temperature range of the studies and slight divergence at higher temperatures, as also observed for the simulations of the current dataset.

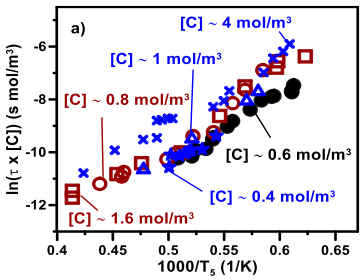

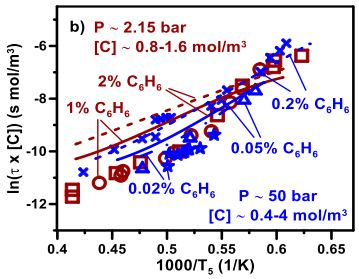

Figure 3. Comparison of literature experiments vs. HST-ICARE data and prediction of soot induction times with current model for pyrolysis of C_6H_6. Literature from: ×, △, ☆ Vlasov [16]; ▱, ○ Drakon [15]; ● HST-ICARE; lines: simulations.

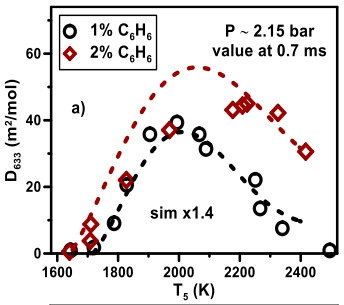

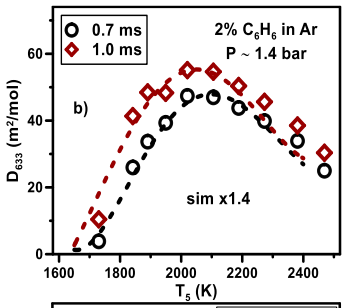

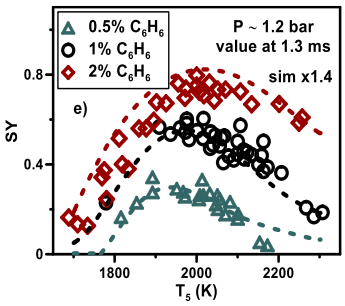

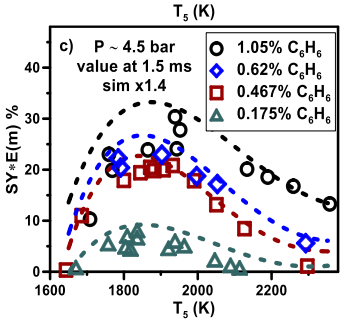

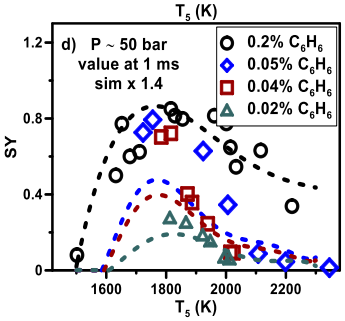

Figure 4. Simulation of literature shock-tube data for benzene pyrolysis. 4a Drakon et al.[15], 4b Natived et al.[17], 4c Agafonov et al. [18], 4d Vlasov et al. [16], 4e Naydenova et al. [19]

Figure 4 shows an overall comparison of model performance against literature datasets of soot volume fractions from benzene pyrolysis at different concentrations. All modeling results were multiplied by a factor of 1.4. The trends are globally well reproduced throughout the entire temperature ranges of the different studies, except for the results presented in Figure 4d, where the model underpredicts the soot volume fractions obtained with initial fuel mole fractions of 0.04% and 0.05%. On the other hand, we notice that these two datasets have similar volume fractions as the ones obtained with 0.2% benzene, an anomaly considering that the soot should increase with increasing initial carbon concentrations. The results in Figure 4 confirm the accuracy of the current modeling approach. Other kinetic analyses will be performed to clarify the pathways to soot formation at the different conditions.

Acknowledgements

This project has received funding from the European Research Council (ERC) under the European Union's Horizon 2020 research and innovation programme (grant agreement No. 756785).

References

[1] Bockhorn, H. A Short Introduction to the Problem. In Soot Formation in Combustion-Mechanisms and Models, Bockhorn H., Ed.; Springer Series in Chemical Physics, Volume 59, 1994, pp 3-9
[2] Lighty, J. S.; Veranth, J. M.; Sarofim, A. F. Combustion aerosols: factors governing their size and composition and implications to human health. J. Air Waste Manage. 2000, 50, 1565-1618
[3] F. Gelbard, J.H. Seinfeld, Simulation of multicomponent aerosol dynamics, J. Colloid Interface Sci. 78 (1980) 485–501
[4] Hamadi, A., Sun, W., Abid, S., Chaumeix, N., Comandini, A., 2022. An experimental and kinetic modeling study of benzene pyrolysis with C2−C3 unsaturated hydrocarbons. Combustion and Flame 237, 111858
[5] Frenklach, M., Taki, S., Durgaprasad, M.B., Soot Formation in Shock-Tube Pyrolysis of Acetylene, Allene, and 1,3-Butadiene, Combust. Flame 54, 81-101
[6] Krestinin, A.V., 1998. Polyyne model of soot formation process. Twenty-Seventh Sysposium (International) on Combustion 27, 1557–1563
[7] De Iuliis, S., Chaumeix, N., Idir, M., Paillard, C.-E., 2008. Scattering/extinction measurements of soot formation in a shock tube. Experimental Thermal and Fluid Science, Fifth mediterranean combustion symposium 32, 1354–1362
[8] Mathieu, O., Djebaïli-Chaumeix, N., Paillard, C.-E., Douce, F., 2009. Experimental study of soot formation from a diesel fuel surrogate in a shock tube. Combustion and Flame 156, 1576–1586
[9] Agafonov, G. L.; Bilera, I. V.; Vlasov, P. A.; Kolbanovskii, Y. A.; Smirnov, V. N.; Tereza, A. M., Soot formation during the pyrolysis and oxidation of acetylene and ethylene in shock waves. Kinet. Catal. 2015, 56, 12
[10] Nativel, D.; Herzler, J.; Krzywdziak, S.; Peukert, S.; Fikri, M.; Schulz, C., Shock-tube study of the influence of oxygenated additives on benzene pyrolysis: Measurement of optical densities, soot inception times and comparison with simulations. Combust. Flame 2022, 111985
[11] Nobili, A., Fanari, N., Dinelli, T., Cipriano, E., Cuoci, A., Pelucchi, M., Frassoldati, A., Faravelli, T., 2024. Kinetic modeling of carbonaceous particle morphology, polydispersity and nanostructure through the discrete sectional approach. Combustion and Flame 269, 113697
[12] A. D'Alessio; A. Barone; R. Cau; A. D'Anna; P. Minutolo, Proceedings of the Combustion Institute 30 (2005) 2595-2603
[13] Cantera is an open-source suite of tools for problems involving chemical kinetics, thermodynamics, and transport processes. https://cantera.org/
[14] https://www.ansys.com/fr-fr/products/fluids/ansys-chemkin-pro
[15] Drakon, A., 2018. Soot formation in shock-wave-induced pyrolysis of acetylene and benzene with H2, O2, and CH4 addition. Combustion and Flame 198, 158–168
[16] Vlasov, P., Warnatz, J., 2002. Detailed kinetic modeling of soot formation in hydrocarbon pyrolysis behind shock waves. Proceedings of the Combustion Institute 29, 2335–2341
[17] Nativel, D., Herzler, J., Krzywdziak, S., Peukert, S., Fikri, M., Schulz, C., 2022. Shock-tube study of the influence of oxygenated additives on benzene pyrolysis: Measurement of optical densities, soot inception times and comparison with simulations. Combustion and Flame, A dedication to Professor Katharina Kohse-Höinghaus 243, 111985
[18] Agafonov, G.L., Smirnov, V.N., Vlasov, P.A., 2011. Shock tube and modeling study of soot formation during the pyrolysis and oxidation of a number of aliphatic and aromatic hydrocarbons. Proceedings of the Combustion Institute 33, 625–632
[19] Naydenova, I., Nullmeier, M., Warnatz, J., Vlasov, P.A., 2004. Detailed Kinetic Modeling of Soot Formation During Shock-Tube Pyrolysis of C6h6: Direct Comparison with the Results of Time-Resolved Laser-Induced Incandescence (lii) and Cw-Laser Extinction Measurements. Combustion Science and Technology 176, 1667
[20] The Homogeneous Pyrolysis of Acetylene II: The High Temperature Radical Chain Mechanism: Combustion Science and Technology: Vol 82, No 1-6